Piotr KISAŁA

Lublin University of Technology, Lublin

Detection of material defects with indirect method by determining the linear expansion with FBG sensor

Streszczenie. *W niniejszym artykule zaprezentowana została metoda wykrywania błędów i defektów w materiałach o znanym współczynniku Younga. Użyty model czujnika FBG (opartego na światłowodowej siatce Bragga), został przetestowany w warunkach laboratoryjnych w procesie diagnozowania różnych defektów na przygotowanych do badań próbkach. Na podstawie dokonanych pomiarów i przeprowadzonych badań, widać w jakim stopniu czujnik optoelektroniczny wykazuje zdolność wykrywania zaburzeń i defektów. Rozdzielczość liniowa pomiaru wydłużenia przy wykorzystaniu zaproponowanej metody wyniosła 1.25 mm. Przeprowadzone badania potwierdziły występowanie defektów, które były rozstawione w odległości 3.14 mm. W przypadku badanych próbek materiału różnice w lokalizacji maksymalnego wydłużenia wyniosły ok. 0.6 mm.* ***(Wykrywanie defektów materiałowych metodą pośrednią poprzez wyznaczenie wydłużeń względnych czujnikiem FBG).***

Abstract*. This paper presents a method of detecting errors and defects in materials with a known Young modulus. The FBG (fiber Bragg grating) sensor used in the model was tested under the laboratory conditions when diagnosing various defects in the samples prepared for testing. Based on the performed measurements and research, the extent of the optoelectronic sensor ability to detect abnormalities and defects was shown. The linear measuring resolution of the expansion with the proposed method was 1.25 mm. The studies confirmed the presence of defects, which were spaced at a distance of 3.14 mm. In the case of samples of material studied, the differences in location of the maximum elongation amounted to approximately 0.6 mm.*

Słowa kluczowe: pomiary wydłużenia liniowego, czujniki defektów materiałowych, pomiary pośrednie, inverse problem.
Keywords: linear expansion measurement, material defects sensors, indirect measurements, problem odwrotny.

Introduction

The demand for circuits and measurement systems that are progressively more accurate, more sensitive, faster and resistant to external interference factors is impacting the optoelectronics development – including the research devoted to designing appropriate components, systems and methods of the cognitive process with using optoelectronic sensors. The systems using fiber optic sensors are the subject of research and development, e.g., acceleration measurement [1], the angle of rotation [2], electric and magnetic fields [3], pressure [4], temperature [5], acoustic wave [6], vibration [7], expansion [8], humidity [9], viscosity [10], the composition of the material [11] and environmental monitoring sensor systems [12].

Noteworthy is also the development of multipoint and distributed fiber optic sensors systems. From the point of view of their possible use in measuring instruments, the sensors based on fiber Bragg gratings [13, 14, 15, 16, 17] constitute a group that is particularly important. In contrast to the photodetector – which is sensitive only to the intensity of light falling on its surface and used as a receiver of light waves – measuring the phase, frequency and polarization of light modulated by the presence of measurand requires interferometric techniques [18] and the use of optical signal processing methods [19].

It is possible to detect defects in the material by – among others – measuring the relative material expansion subjected, for example, to tensile force. The linear stress differences appearing along the length of the measurement can be used as the indication of deformations and defects in the material. Determining the non-uniform distribution of the relative expansion of the material is an example of drawing conclusions about the reasons based on the effects. Such process is called the inverse problem [20]. The inverse problem, therefore, occurs as a result of the need to determine the quantitative distribution of the relative expansion (cause) with a known form of the transmission spectrum of the system (effect) achieved through building the sensor model. In this paper, the inverse problem was applied to estimate the parameters of a sensor model of the relative expansion distribution. The described method does not take into account changes in temperature and therefore is not immune to such changes. From a practical point of view, it seems reasonable, therefore, to implement a mechanism that allows becoming independent of temperature changes, for example, using the second Bragg grating [21]. Exclusion of the temperature changes also facilitates neglecting the issue of regularization when solving the inverse problem [22, 23].

In the majority of studies the grating is fixed using epoxy glue [24]. Also, the FBG sensors are usually mounted in a variety of complex composite materials [25]. In our study, the gratings are glued on metal surface of samples using an adhesive with a high Young modulus, which increases the transmission rate of the expansion of the test sample to the FBG element. Such solution allows for easy mounting of the sensors in the prospective measurement systems.

Method of detecting material defects using periodic structures of fiber optics

The proposed method is based on indirect measurements – relative expansions, with optoelectronic sensor and a transmitter in the form of a uniform Bragg grating. The problem was brought up to determine the relative expansion distribution function $\varepsilon(z)$ along the grating axis, based on the grating reflection spectrum, measured and designated as $P_R(\lambda)$.

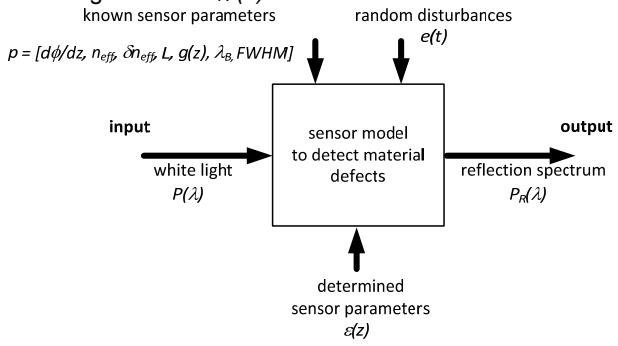

Fig. 1. System block diagram with the sensor model and the known and determined parameters

To solve the problem, a mathematical model of the sensor was built based on a uniform Bragg grating that includes mathematical relations, enabling to correlate a

directly measured reflection spectrum $P_R(\lambda)$ of the relative expansion distribution $\varepsilon(z)$ that is sought. The model block diagram is shown in Figure 1.

The model used the processing function of the white-light acting as the input signal at the known sensor parameters, such as grating chirp $d\phi/dz$, apodized profile $g(z)$ [11], sensor resonant wavelength λ_B, the full width at half maximum (*FWHM*) of sensor reflection characteristics occurring in the absence of stress, the length of the grating L, amplitude modulation of the grating refractive index δn_{eff}, the effective grating refractive index n_{eff} and other. To build the sensor model, a discrete transfer matrix method was used [26].

To assemble a measuring system to detect material defects, it was necessary to build a non-uniform grating model as defects result in the occurrence of non-uniform stress along the Bragg grating length. In the case of non-uniform gratings, it is difficult to find an analytical solution to coupled modes equations and so such equations can be solved by numerical methods. The paper makes the assumption that the refractive index modulation that is formed is approximately uniform across the entire Bragg grating located in the fiber core. Also assumed was the lack of modes propagating outside the core. Thus, in a further mathematical analysis, cladding modes can be abandoned. The electric field distribution along the core of the fiber can thus be expressed as follows [27]:

$$E(x,y,z)=\left[A(z)\exp(-i\beta z)+B(z)\exp(-\beta z)\right]e_t(x,y), \tag{1}$$

where $A(z)$ and $B(z)$ are the amplitudes of modes propagating respectively in the directions +z (positive – from the grating input to output), and -z (negative – from the grating output to the input), e_t is the transverse mode field, while the propagation constant β is equal to

$$\beta=(2\pi/\lambda)n_{eff}, \tag{2}$$

where n_{eff} is the effective grating refractive index, while λ is the wavelength. Now let's introduce the $E(x, y, z)$ distribution to the coupled modes equations. We then obtain the equations of mode fields propagating in the positive $R(z)$ and negative $S(z)$ directions:

$$\frac{dR(z;\delta)}{dz}=+i\delta(z)R(z)+q(z)S(z), \tag{3}$$

$$\frac{dS(z;\delta)}{dz}=-i\delta(z)S(z)+q^*(z)R(z), \tag{4}$$

where δ is a detuning parameter of the resonance wavelength frequency (Bragg wavelength) and is expressed as

$$\delta=\beta-\frac{\pi}{\lambda}=2\pi n_{eff}\left(\frac{1}{\lambda}-\frac{1}{\lambda_B}\right), \tag{5}$$

Value of q is called a slowly varying complex coupling coefficient and is equal to:

$$q=i\kappa, \tag{6}$$

Note that each pair of $\{R(z), S(z)\}$ solutions of the coupled modes equations must satisfy the equations (3) and (4) with two boundary conditions (7) and (8):

$$\begin{aligned} R(0;\delta)&=1\\ S(L,\delta)&=0 \end{aligned}, \tag{7}$$

for which the reflection sensor is equal to $P_R(\delta) = S(0, \delta)$, while the sensor transmission is $P_T(\delta) = R(L; \delta)$. The L symbol denotes the grating length. To determine the grating reflection spectrum (model output) the model was divided into discrete series of finite Bragg reflectors. In contrast to the tranfer matrix method [28], in this paper the entire grating was divided into discrete string of Bragg reflectors connected serially to one another. Hence, equation (8) describing the signal at the ends of the grating:

$$\begin{bmatrix}R(L)\\S(L)\end{bmatrix}=\mathbf{T}\begin{bmatrix}R(0)\\S(0)\end{bmatrix}, \tag{8}$$

where **T** is the matrix that describes the transition function of the grating, can now be written as:

$$\begin{bmatrix}R(L)\\S(L)\end{bmatrix}=\begin{bmatrix}e^{(i\delta\Delta z)} & 0\\ 0 & e^{-(i\delta\Delta z)}\end{bmatrix}\begin{bmatrix}1 & -r_k^*\\ r_k & 1\end{bmatrix}\left(1-|r_k|^2\right)^{-\frac{1}{2}}\begin{bmatrix}R(0)\\S(0)\end{bmatrix}, \tag{9}$$

Element $\begin{bmatrix}e^{(i\delta\Delta z)} & 0\\ 0 & e^{-(i\delta\Delta z)}\end{bmatrix}$ denotes the matrix of sensor propagation, while the matrix of one discrete Bragg reflector is expressed by the factor $\begin{bmatrix}1 & -r_k^*\\ r_k & 1\end{bmatrix}$ and Δz denotes the length of one discrete Bragg reflector. The reflection of such one reflector is expressed by the relation

$$r_k=-\tanh\left(|q_k|\Delta z\right)q_k^*/|q_k|. \tag{10}$$

Thus we will express the entire sensor reflection as:

$$\begin{aligned} P_R(z;\delta)&=\left[\rho_k+P_R(z+\Delta z;\delta)e^{2i\delta\Delta z}\right]\\ &/\left[1+\rho_k^*P_R(z+\Delta z;\delta)e^{2i\delta\Delta z}\right] \end{aligned}, \tag{11}$$

Reflection of the entire sensor was obtained under the assumption that $P_R(L; \delta) = 0$, taking into account equation (11), up to $z = 0$, to obtain the spectrum $P_R(\delta) = P_R(0; \delta)$. For each discrete section, $P_R(z; \delta)$ reflection is calculated resulting from the signal propagation by the different Bragg reflectors that constitute the entire sensor

A mathematical model of the reflective spectrum measurement was formulated in the general form of Fredholm integral equation of the first kind [23]:

$$P_R(\lambda)=K[\varepsilon(z)]=\int_{z_{\min}}^{z_{\max}}K(\lambda,z)\varepsilon(z)dz, \tag{12}$$

while:

$$\lambda_{\min}\le\lambda\le\lambda_{\max}, \tag{13}$$

In equation (12), $K(\lambda, z)$ is a function of the kernel. The inverse problem will be to designate the function $\varepsilon(z)$ based on the relation measurement $P_R(\lambda)$, using a mathematical model and the expansion measurements data of the apodized Bragg grating, with the sensor and the transmitter of a homogeneous nature. The inverse problem of indirect measurements of relative expansion with FBG sensor, defined as the solution to Fredholm equation written as (12) will depend on determining the grating parameters on the basis of the reflection spectrum. These parameters are values of the relative expansion, which was designated as ε. This determination can be made by measuring the reflected power distribution frequency of the sensor. This distribution was designated as $P_R(\lambda)$. The measurement data, thus determined by $P_R(\lambda)$ value, are then measured using direct measurement with the optical spectrum analyzer. The function ε mapping the relative expansion to the reflection power K will be expressed as:

(14) $$P_R = K(\varepsilon) = K\varepsilon ,$$

In order to solve such problem, it is necessary to use iterative methods and inverse problem discretization. Figure 2 shows a block diagram of the algorithm used to validate the model of the sensor:

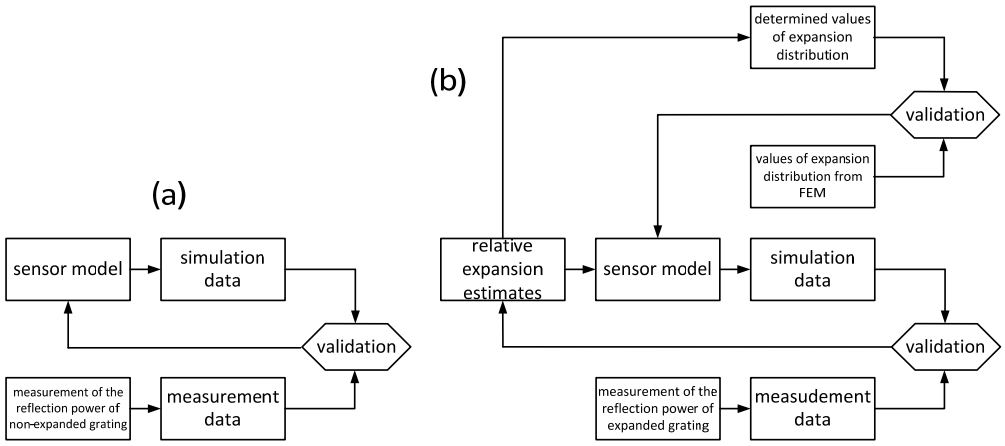

Fig. 2. Block diagram showing algorithms of (a) – initial validation and (b) – proper validation of the sensor model

Validation of the sensor model proceeded in two stages. In the first stage (Fig. 2a), the data obtained using the expansion distribution sensor model (simulation data – the modeled sensor reflection spectrum) was compared with the data obtained during measurements (measured reflection characteristics of the sensor). Validation enabled the appropriate update of the sensor parameters at the state without stress. In the second stage (Figure 2b) a so-called proper validation of the sensor model was performed. Expansion distribution estimates were used as the model input. Based on that, the model characteristics (simulation data) were obtained, which were then compared with the measured data from the sensor under stress. Once the consistency of simulation and measurement data was determined, the relative expansion values obtained by validation were compared with the values obtained from the finite element method, and the differences between them were used to update and correct the parameters of the sensor model.

Laboratory tests

In the laboratory experiment, tests were performed on a specially manufactured steel samples with a value of Young modulus E = 204.5 GPa, with specially prepared defects produced with laser. To produce such defects, the CO_2 resonator laser (TRUMPF TC L 4030) was used, which produces a beam with a very small angle of divergence and shape of the cutting radius.

Energy distribution of the beam resembles a bell-shaped curve. The power density reaches 10^7 W/cm^2 at the focus point. Such power value and beam shape allow for the precise completion of the desired shape of defects in the test sample. Figure 3 shows a sample implementation and heterogeneity.

In addition, in experimental studies a Bragg grating with Bragg wavelength equal to 1551.5 nm was used – written on hydrogenated singlemode fiber using the phase mask, allowing for its apodization in accordance with the profile in the shape of Gaussian function. Grating of the length *L* = 15 mm was attached to the metal sample using Sikadur-30 adhesive. Samples and the "defect-fault" shapes used for test are shown in Figure 4.

Samples 2a and 2c are made with the same irregular defect (star shape) – but oriented so as to obtain a single notch and the double notch effect. A sample with the star arms positioned perpendicularly to the fiber optic (2a) – single notch, and the sample with the star arms rotated by the value of arm marker – double notch (2c). The third sample (2b) has a regular (circular) shape. The dimensions of the samples and defects are shown in Figure 5.

Note that in the case of irregularly shaped defects in the form of a star with the arm perpendicular to the fiber optic axis, a single notch effect is triggered, while for the case of the star with the rotated arm – the notch is multiple, not single.

By analyzing the relative performance of linear expansion (Figs. 6, 7 and 8) calculated during the simulation by the finite elements method with the characteristics obtained using the proposed method, we can see their high level of coverage. As can be seen in all tested samples, reaction that occurs depends on the type of the defect.

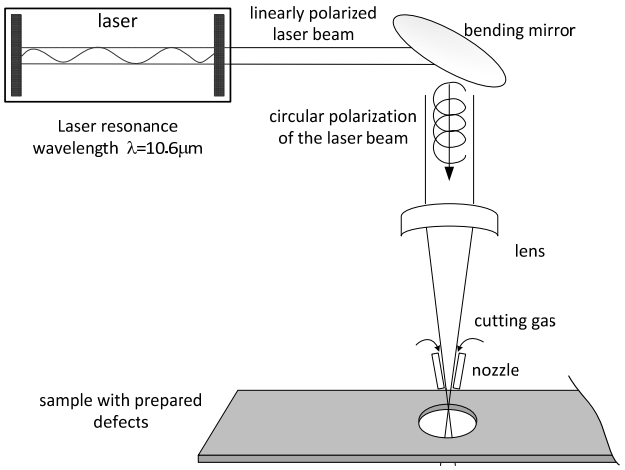

Fig. 3. Method of preparing defects in the tested material using the CO_2 resonator laser

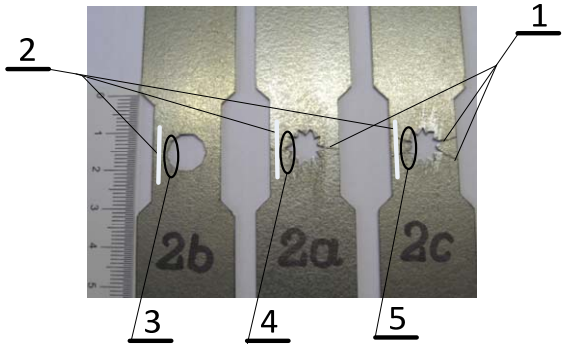

Fig. 4. Method of preparing defects in the tested material using the CO_2 resonator laser. The figure designations are as follows: 1 – star arms axes, 2 – sensor location, 3 – area without notch, 4 –area of single notch effect, 5 –area of double notch effect

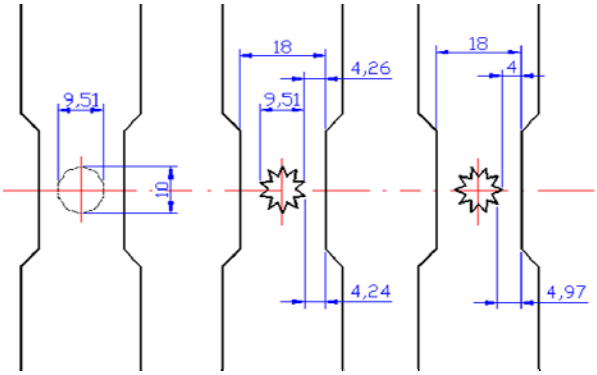

Fig. 5. Dimensions of the material defects tested

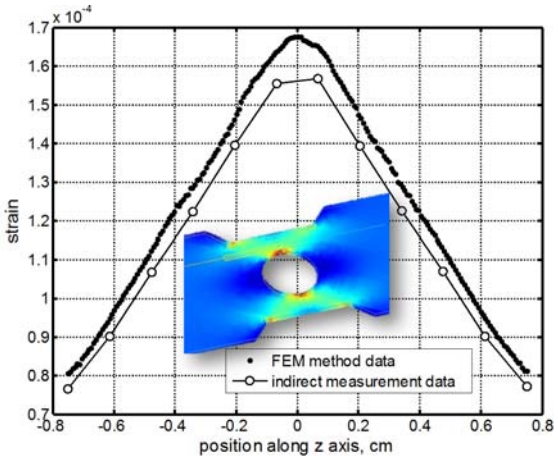

Fig. 6. Values of relative expansion calculated with the finite elements method (FEM) and those obtained with the proposed method of intermediate measurement. Results obtained for sample 2b in Fig. 4

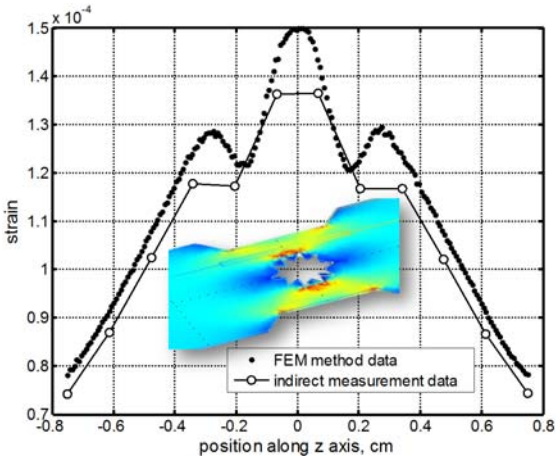

Fig. 7. Values of relative expansion calculated with the finite elements method (FEM) and those obtained with the proposed method of intermediate measurement. Results obtained for sample 2c in Fig. 4.

A very important element is the ability to determine the maximum expansion of the tested material or location where the stress has the highest values. In the case of material samples, differences in locations of the maximum expansion amounted to approximately 0.6 mm.

For the results for the samples shown in Figures 6 and 7, the measured values of the maximum relative expansion occur for the same positions along the z-axis for the values determined by FEM method. As can be seen from Figures 6, 7 and 8, the expansion values were determined at 12 points, which, at the gauge length equal to 15 mm gives a linear resolution of the expansion measurement equal to 1.25 mm. The conducted experimental studies confirmed the presence of defects, which were spaced at a distance of 3.14 mm (for both single and multiple notches). Spectral characteristics on which the waveforms in Figs. 6, 7 and 8 were determined, also show a high sensitivity to the nature of the deformation which suggests that defects with smaller physical sizes could also be detected by this method.

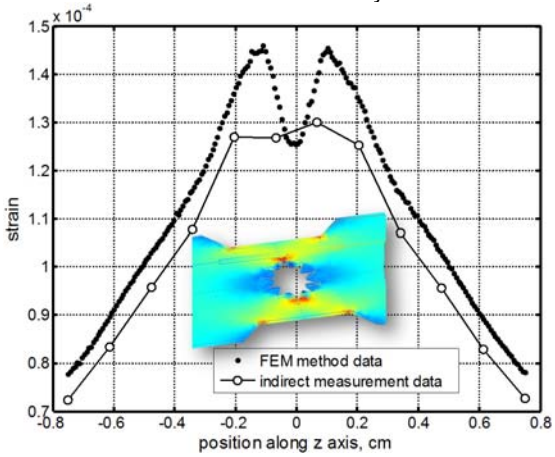

Fig. 8. Values of relative expansion calculated with the finite elements method (FEM) and those obtained with the proposed method of intermediate measurement. Results obtained for sample 2a in Fig. 4.

Conclusions

This paper presents a method for detecting faults and defects in materials with a known Young modulus. Tests have confirmed the ability to distinguish between defects with the size of only a few millimeters. A high level of linear expansion characteristics coverage obtained with FEM with the waveforms derived from indirect measurements confirm the applicability of the proposed method for the analysis of defects of other shapes, but similar physical size. An important feature of the described methods is also a capability to determine the nature of the changes in the material expansion. The resolution of defects measurements with application of the proposed algorithm was 1.25 mm. The presented method for detecting defects thus provides features which may be useful in the measuring process.

REFERENCES

[1] Xiao G., Long X., Zhang B., Jin S., A novel active optical approach for acceleration measurement based on aY-shaped cavity dual-frequency laser, Optics & Laser Technology, Vol. 44 (2012) s. 344–348.

[2] Cavallo A., De Maria G., Natale C., Pirozzi S., Optoelectronic joint angular sensor for robotic fingers, Sensors and Actuators A, Vol. 152 (2009) s. 203–210.

[3] Davino D., Visone C., Ambrosino C., Campopiano S., Cusano A., Cutolo A., Compensation of hysteresis in magnetic field sensors employing Fiber Bragg Grating and magneto-elastic materials, Sensors and Actuators A, Vol. 147 (2008) s. 127–136.

[4] Lei K.F., Lee K.-F., Lee M.-Y., Development of a Flexible PDMS Capacitive Pressure Sensor for Plantar Pressure Measurement, Microelectronic Engineering 99 (2012) 1–5.

[5] Wen X., Zhang D., Qian Y., Li J., Fei N., Improving the peak wavelength detection accuracy of Sn-doped, H2-loaded FBG high temperature sensors by wavelet filter and Gaussian curve fitting, Sensors and Actuators A, Vol. 174 (2012) s. 91– 95.

[6] Furstenau N., Schmidt M., Horack H., Goetze W., Schmidt W., Extrinsic Fabry-Perot interferometer vibration

and acoustic sensor systems for airport groung traffic monitoring, IEE Proc -Optoelectron, Vol. 144, No 3 (1997), s. 134-144.
[7] Bin M., Jian X., Experimental Research of Coupling Fiber-optic Sensor for Vibration Measurement, IEEE (2010) s. 1-4.
[8] Yuan L., Zhou L., Jin W., Fiber Optic Differential Interferometer, IEEE TRANSACTIONS ON INSTRUMENTATION AND MEASUREMENT, Vol. 49, No. 4 (2000) s. 779-782.
[9] Consales M., Buosciolo A., Cutolo A., Breglio G., Irace A., Buontempo S., Petagna P., Giordano M., Cusano A., Fiber optic humidity sensors for high-energy physics applications at CERN, Sensors and Actuators B, Vol. 159 (2011) s. 66– 74.
[10] Wang W.-C., Yee S.S., Reinhall P. G., Optical viscosity sensor using forward light scattering, Sensors and Actuators B, 24-25 (1995) s. 753-755.
[11] Wójcik W., Cięszczyk S., Kisała P., Wykorzystanie informacji o drugiej pochodnej widma w iteracyjnych algorytmach rekonstrukcji widm w spektroskopii, Przegląd Elektrotechniczny, No 10 (2010) s. 143-146.
[12] Hotra Z., Mykytyuk Z., Sushynskyy O., Hotra O., Kisała P., Systemy sensorowe z optycznym kanałem przesyłu informacji, Przegląd Elektrotechniczny, No 10 (2010) s. 21-23.
[13] Liu H., Or S.W., Tam H.Y., Magnetostrictive composite–fiber Bragg grating (MC–FBG) magnetic field sensor, Sensors and Actuators A, Vol. 173 (2012) s. 122–126.
[14] Kisała P., Application of inverse analysis to determine the strain distribution with optoelectronic method insensitive to temperature changes, Applied Optics, Vol. 51 Issue 16 (2012) s. 3599-3604.
[15] Wójcik W., Kisała P., WYBRANE ZASTOSOWANIA CZUJNIKÓW OPTOELEKTRONICZNYCH, Elektronika, nr 7 (2009) s. 181-189.
[16] Sohn K.-R., Fiber Bragg grating-tuned feedback laser flow sensor system, Sensors and Actuators A 179 (2012) 1– 4.
[17] Sanada H., Sugita Y., Kashiwai Y., Development of a multi-interval displacement sensor using Fiber Bragg Grating technology, International Journal of Rock Mechanics & Mining Sciences, Vol. 54 (2012) s. 27–36.
[18] Yuan L.-B., Multiplexed &ber optic sensors matrix demodulated by a white light interferometric Mach–Zehnder interrogator, Optics & Laser Technology, Vol. 36 (2004) s. 365–369.
[19] Gordon R.P., Lautz L.K., Briggs M.A., McKenzie J.M., Automated calculation of vertical pore-water flux from field temperature time series using the VFLUX method and computer program, Journal of Hydrology Vol. 420–421 (2012) s. 142–158.
[20] Mroczka J., Szczuczyński D., Inverse problems formulated in term of first-kind fredholm integral equations in indirect measurements, Metrol. Meas. Syst. Vol. XVI, No 3 (2009) s. 333-357.
[21] Piotr Kisała : Optoelektroniczny czujnik do równoległego i niezależnego pomiaru temperatury i wydłużenia wykorzystujący światłowodowe siatki Bragga, Przegląd Elektrotechniczny, No. 11a (2012), 343-346
[22] Mroczka J. Szczuczyński D., Simulation research on improved regularized solution of the inverse problem in spectral extinction measurements, Applied Optics, Vol. 51, Issue 11 (2012) 1715-1723.
[23] Mroczka J., Szczuczyński D., Improved regularized solution of the inverse problem in turbidimetric measurements, Appl. Opt. Vol. 49 (2010) s. 4591-4603.
[24] Botsis J., Humbert L., Colpo F., Giaccari P., Embedded fiber Bragg grating sensor for internal strain measurements in polymeric materials, Optics and Lasers in Engineering 43 (2005) 491–510.
[25] Kuang K. S. C., Kenny R., Whelan M. P., Cantwell W. J., Chalker P. R., Embedded fibre Bragg grating sensors in advanced composite materials, Composites Science and Technology 61 (2001) 1379–1387.
[26] Yamada M. Sakuda K., Analysis of almost-periodic distributed feedback slab waveguides via a fundamental matrix approach, Applied Optics, Vol. 26, No. 16 (1987) s. 3474-3478.
[27] Bao J., Zhang X., Chen K., Zhou W., Spectra of dual overwritten fiber Bragg grating, Optics Communications 188 (2001) 31-39.
[28] Chena Y, Li J., Yanga Y., Chena M., Li J., Luo H., Numerical modeling and design of mid-infrared FBG with high reflectivity, Optik (2012) (in press).

***Authors**: dr inż. Piotr Kisała, Politechnika Lubelska, Instytut Elektroniki i Technik Informacyjnych, ul. Nadbystrzycka 38A, 20-618 Lublin, E-mail: p.kisala@pollub.pl*.